Histol Histopathol (2009) 24: 1275-1286

http://www.hh.um.es

Histology and Histopathology

Cellular and Molecular Biology

Mitochondrial bioenergetics and distribution in living human osteoblasts grown on implant surfaces

Mercedes Salido[1], J. Ignacio Vilches-Perez[2], Juan L. Gonzalez[3] and Jose Vilches[1]

[1]Department of Histology, School of Medicine, Laboratory 57, Servicios Centrales de Investigación en Ciencias de la Salud, University of Cadiz, Cadiz, Spain, [2]Department of Oral surgery, School of Dentistry. University of Seville, Seville, Spain and [3]Department of Statistics and Operational Research, School of Medicine, University of Cadiz, Cadiz, Spain

Summary. Osseointegration of implants is crucial for the long-term success of oral implants. The periimplant bone formation by osteoblasts is strongly dependent on the local mechanical environment in the interface zone. Robust demands for energy are placed on osteoblasts during the adhesion process to solid surfaces, and mitochondria are capital organelles in the production of most of the ATP needed for the process. We have assessed the relationship between osteoblast differentiation and mitochondrial bioenergetics in living cells grown on two different titanium surfaces, in order to provide valuable information for the design of material surfaces required for the development of the most appropriate osteogenic surface for osteoblastic anchorage. Combined backscattered and fluorescence confocal microscopy showed that in flat cells grown on a machined surface, highly energized mitochondria were distributed along the cell body. In contrast, cells grown on the rough surface emitted long protrusions in search of surface roughness, with actin stress fibers clearly polarized and highly energized mitochondria clustered at focal adhesion sites. This report using normal human osteoblastic cells indicates that these cells are especially sensitive to surface cues through energy production that enhances the necessary adhesion required for a successful osseointegration.

Key words: Titanium, Surface topography, Osteoblast, Cell adhesion, Mitochondrial membrane potential

Offprint requests to: Mercedes Salido, Department of Histology, School of Medicine, Laboratory 57, Servicios Centrales de Investigación en Ciencias de la Salud, University of Cadiz, C/ Dr. Marañon 3, 11002 Cádiz. Spain. e-mail: mercedes.salido@uca.es

Introduction

Recent research has suggested that bones display an extraordinary adaptative behaviour towards changing mechanical environment, which is often regarded as phenotype plasticity. Furthermore, the periimplant tissue formation and mineralization by osteoblasts are strongly dependent on the local mechanical environment in the interface zone. The quality of cell adhesion to the implant surface determines tissue integration, and the surface roughness can directly influence osteoblast adherence, attachment, spreading and metabolism modifying and controlling the osseointegration process (Pierres et al., 2002; Ingber, 2003a,b; Sader et al., 2005; Chiesa et al., 2007; Gatti et al., 2008).

In migrating cells, actin filaments are primarily organized into submembrane meshworks that appear diffuse or in small bundles, whereas stationary cells usually display conspicuous arrays of filament bundles, "stress fibers", which are anchored at their termini in matrix attachments known as focal adhesions (Chen et al., 2003; Zimerman et al., 2004; Diener et al., 2005; Hu et al., 2007). Robust demands for energy are placed on osteoblasts in the adhesion process to solid surfaces, and mitochondria are responsible for the production of the largest part of cellular ATP needed for endoergonic processes within the cell (Grigoriou et al., 2005; Anesti and Scorrano, 2006; Boldogh and Pon, 2007).

To understand how microtopography modulates cell adhesion, in the present study we have developed an in vitro model, using the human osteoblastic cell line NHOst®, to study mitochondrial distribution and bioenergetics during the initial phases of the adhesion process to different titanium implant surfaces, prepared as disks for in vitro manipulation .

There is a direct correlation between the energized state of mitochondria and the mitochondrial membrane ($\Delta\psi\mu$) when analyzed in isolated mitochondria (Salvioli

et al., 1997; Dedov and Roufogalis, 1999, Salido et al., 2007a). In order to provide valuable information for the design of material surfaces that are required for the development of the most appropriate osteogenic surface for osteoblastic anchorage in dental implants, the relationship between osteoblast differentiation on different titanium surfaces and cellular bioenergetics has been assessed in living cells in this study, by means of combined backscattered and fluorescence analysis with confocal microscopy. Thus, the dynamics of a physiological process, as is the case for the initial phases of osseointegration, can be determined. We have, thus, used this information to reconstruct the three-dimensional interface between the osteoblastic cells and the implant surface.

The results presented herein enforce the role of the rough substratum surface in affecting osteoblastic cell adhesion, required for the development of an appropriate osteogenic surface for osteoblastic anchorage and maturation, compared to a machined surface in dental implants.

Material and methods

To evaluate the relationship between osteoblast differentiation and bioenergetics, NHOst cells were grown on different titanium surfaces, Ti CP machined and Ti CP Osseotite®, provided as prefabricated 2 cm x 1.5 mm disks, in medium supplemented with ascorbate to induce differentiation. To evaluate changes in mitochondrial membrane potential ($\Delta\psi\mu$)) and in subcellular distribution in response to different scaffolds, cells were stained with a transmembrane potential-sensitive vital dye, JC1, which preferently accumulates in mitochondria by $\Delta\psi\mu$ dependent mechanism, and confocal imaged. Actin cytoskeletal organization was assessed by immunostaining with rhodamine phalloidin in order to study the role of the substratum surface in affecting osteoblastic cell adhesion.

Cell culture

Normal human osteoblastic NHOst® cells (Cambrex, Walkersville, MD, USA) were seeded at a density of 5000 cells/cm^2 and incubated in Osteoblast Growing Medium, OGM, (Cambrex, Walkersville, MD, USA) containing 10% fetal bovine serum (Cambrex, Walkersville, MD, USA), 1% gentamycin sulphate/ amphotericin B (Cambrex, Walkersville, MD, USA) and 1% ascorbic acid (Cambrex, Walkersville, MD, USA), as recommended by suppliers, at 37°C and 5% CO_2 until the experiments started. Growth medium was changed daily after seeding. Before the cells became 80% confluent they were subcultured with 2 ml of 0.25 mg/ml trypsin EDTA warmed to 37°C (Cambrex, Walkersville, MD, USA) after rinsing with 5 ml Hepes-BSS (Cambrex, Walkersville, MD, USA) at room temperature. Once cells were detached, trypsin EDTA was neutralized by adding 4 ml of trypsin neutralizing solution (Cambrex, Walkersville, MD, USA). Harvested cells were seeded on the different disks at a density of 5000 cells/cm^2 and immunostained after 48 h. Growth medium was changed every day until the experiments were over. NHOst cells are assured for experimental use for ten population doublings, which were not exceeded during the assay.

Titanium disks

Before use, the disks were immersed in 100% ethanol for 10 min, air dried, and exposed under u.v. light for 30 min on each side, and finally rinsed in endotoxin free phosphate buffered solution, and deposited on small sterile Petri dishes prior to cell seeding. Tissue culture Willco® (WillCo Wells, Amsterdam, The Netherlands) wells, with a 0.17 mm glass bottom, were used as the control surface.

Immunohistochemistry and cytoskeletal organization

At the end of the specific culture time, cells were washed twice with prewarmed phosphate-buffered saline, (PBS), pH 7.4, fixed with 3.7% para-formaldehyde (PFA) solution in PBS for 10 min at room temperature, and washed twice with prewarmed PBS. The cells were then permeabilized with 0.1% Triton x-100 (Sigma, St Louis, Missouri, USA) for 5 min and washed twice with prewarmed PBS. To reduce non-specific background staining, 1% bovine serum albumine (BSA) in PBS was added to the surfaces for 20 min, and cells were immunostained for 20 min. with rhodamine phalloidin, 12.5 µl of methanolic stock solution (Sigma, St Louis, Missouri, USA) in 500 µl PBS for each sample. After discarding the staining solution, disks were rinsed with prewarmed PBS three times prior to mounting with vectashield® (Vector Labs. Burlingame CA, USA) and 0.17 mm coverslip in one holed polycarbonate slide devices specially designed in our laboratory and fabricated by means of control precision systems (Mecaprec, Cadiz, Spain).

Mitochondrial permeability potential

Cells were stained with the cationic dye JC-1 (Mito PT TM®, Immunohistochemistry Technologies, Bloomington, MN, USA), which exhibits potential-dependent accumulation in mitochondria. At low membrane potentials, JC-1 continues to exist as a monomer and produces a green fluorescence (emission at 527 nm). At high membrane potentials, JC-1 forms “J-aggregates" (emission at 590 nm) and produces a red fluorescence.

Cells were cultured in Willco® wells with glass bottom as control group for the assay, and on the different disk surfaces provided, not exceeding a final number of 10^6 cells/ml, and after discarding the culture medium, 1x MitoPT® staining solution obtained from a 100x stock was added to the wells, 0.5 ml per well. Cells were then incubated at 37°C for 15 min in a CO_2 incubator and, after discarding the medium, washed

twice with 1-2 ml of assay buffer warmed to 37°C. After discarding the wash, a drop of assay buffer was added to the specimens prior to immediate examination in the inverted confocal microscope Leica TCS SL (Leica, Darmstaad, Germany), equipped with an HCX PL APO CS 63.0x1.30 glycerol immersion objective, with an incubation system consisting of a cube that completely covers the microscope and allows us to keep cells at 37°C in a controlled atmosphere with a mixed air/CO_2 low of 4 l/h and 5% CO_2 during image collection and analysis.

Confocal examination. Image collection and analysis for cytoskeleton

The cells and disks were simultaneously visualized using a Leica TCS-SL confocal microscope equipped with a 63.0x1.30 glycerol objective, allowing simultaneous acquisition of rhodamine phalloidin staining of actin cytoskeleton (excitation 554 nm / emission 573 nm) and surface reflectance. At least four isolated disks were analyzed in each group for profilometric information, and a minimum of four disks with cells growing on them were analyzed in each group, in order to assess surface influence on cytoskeletal organization and cell morphology. At least 50 cells per disk were analysed. Images were collected and processed for quantitative analysis using the imaging software provided by the Leica TCS SL system. Profilometric studies, for the quantification of maximal and minimal values in surface profile, distance between peaks in each surface and width of grooves and valleys in the different surfaces were assessed.

All samples were exposed to laser for a time interval not more than 5 min to avoid photobleaching. The excitation beam splitter selected was a DD 488/543. The laser was set to the lowest power able to produce a fluorescent signal. Maximum voltage of photomultipliers was used to decrease the required laser power as much as possible. Offset was maintained at 0. A pinhole of 1 Airy unit was used. Images were acquired at a resolution of 1024x1024. Series were acquired in the xyz mode.

Image collection and analysis for $\Delta\psi\mu$

The cells and disks were simultaneously visualized using a Leica TCS-SL confocal microscope equipped with a 63.0x1.30 glycerol objective, under the conditions described above, allowing simultaneous acquisition of surface reflectance and JC1 stained mitochondria. JC-1 was excited at 490 nm and the emission fluorescence was collected in TRITC (590 nm) and FITC (530 nm) channels simultaneously.

For quantitative analysis, at least 120 regions of interest (ROIs) were selected in each group to quantify changes in $\Delta\psi\mu$. All of the ROIs are cells selected under the following criteria: well-defined limits, clear identification of nucleus and absence of intersection with neighbouring cells. Size, number of pixels and fluorescence intensity in the red (high membrane potential) and green (low membrane potential) channels in each ROI were calculated.

Statistical analysis

The statistical analysis was performed with SPSS program. A one-way ANOVA analysis was used to compare the mean values for cell areas and red pixel intensity, standard deviation and skewness. The normality of the groups was contrasted with Kolmogorov-Smirnov test and the variances homogeneity with Cochran's C test. Post-hoc contrasts, HSD test of Tukey, were carried out to detect the differences between groups. A value of $p \leq 0.05$ was considered significant.

Results

CLSM characterization of surfaces

Confocal backscattered imaging of disk surfaces, obtained by reflection of the 488 laser line, showed a markedly irregular surface in the TiCP Osseotite® with prominent peaks and caves, as shown (Fig. 1A). Some of them presented well-defined contours, while some others formed a wide trabecular surface with numerous crater-like structures and randomly distributed cavities and borders. The TiCP machined surface displayed parallel grooves, caused by the waviness inherent to the machining operation, which determined a relatively smooth surface (Fig. 1C). Three dimensional reconstructions, obtained from serial acquisition of stacks, were performed for the assessment of osteoblast-surface interface (Fig. 1B,D). The profilometric measurement resulted in a minimum value of 1.2 µm for the depth of the valleys and a maximum value of 4.15 µm for the top of the embossed structure. The mean distance between tops reached 18.28 µm, the mean width for the valleys was 2.85 µm, the mean value found for the groove on top of each embossed ring was 1.51 µm. Ti CP Osseotite® disks showed a marked increase in the surface roughness, with prominent peaks and caves, some of them with well-defined contours and some others forming a wide trabecular surface with randomly distributed peaks. The distance between peaks, consequently, was highly variable, with values ranging from 24.45 µm up to 183.67 µm. The mean diameter of the caves was found to be largely variable, ranging from 8.01 and 39.27 µm. As revealed in the profilometric study, this pattern notably increased the mean roughness of the surface, that showed a minimum value of 1.9 µm in depth and a maximum peak value of 8.79 µm.

CLSM observation of differences in osteoblast phenotypes on different surfaces

Cells growing on the TiCP Osseotite® surface, where the distance between peaks increases, presented an increasingly polarised spreading with emission of either wide lamellipodia or long filopodia, depending on

the surface roughness and the distance between subjacent peaks, and showed the longest morphology with a mean axial ratio that rose to 3.5 (Fig. 2). The actin cytoskeleton adopted an organization characterized by actin bundles running either perpendicularly or slightly obliquely, with apparently segmented contractile units defined topographically by anchorage points, organized according to the surface structure. Parallel actin filaments were observed along the cellular processes and anchoring to focal contacts to relative topographical peaks was observed. As shown, cells clearly fitted to surface topography and even emitted long filopodial branches, when necessary, for successful anchorage mediated by actin "stress fibers" and focal adhesion contacts on selected peaks.

When osteoblasts growing on TiCP machined surfaces were examined, significant differences were observed, not only regarding size and shape, but also to cytoskeletal organization. Cells grown on Ti CP machined surfaces flattened and adopted a largely radial morphology, and appeared to be predominantly planar and randomly oriented with a mean axial ratio of 1.1 (Fig. 3). Cells anchored to the surface by displaying long dendritic filopodia, both along the grooves and crossing over them in a perpendicular way.

Control cells, growing on the glass surface, did not show a patterned morphology. Instead, a number of cells showed long, thin filopodia, while some others flattened and spread over the glass surface, thus presenting a high variability in actin cytoskeleton organization, with actin fibers that appeared running in all directions (Fig. 6D).

Mitochondrial bioenergetics and distribution

On TiCP Osseotite® surfaces, NHOst® cells presented a high density of filamentous mitochondria. Most of the highly energized mitochondria, stained in red (Fig. 4), accumulated in the long filopodial branches. The simultaneous visualization of mitochondrial labelling and the backscattered imaging of the surface allowed us to correlate the mitochondrial distribution with the irregular substratum microtopography, full of peaks and caves, thus confirming mitochondrial polarization to the selected anchorage points.

In cells growing on TiCP machined surfaces, highly energized mitochondria filled the cell body (Fig. 5). No

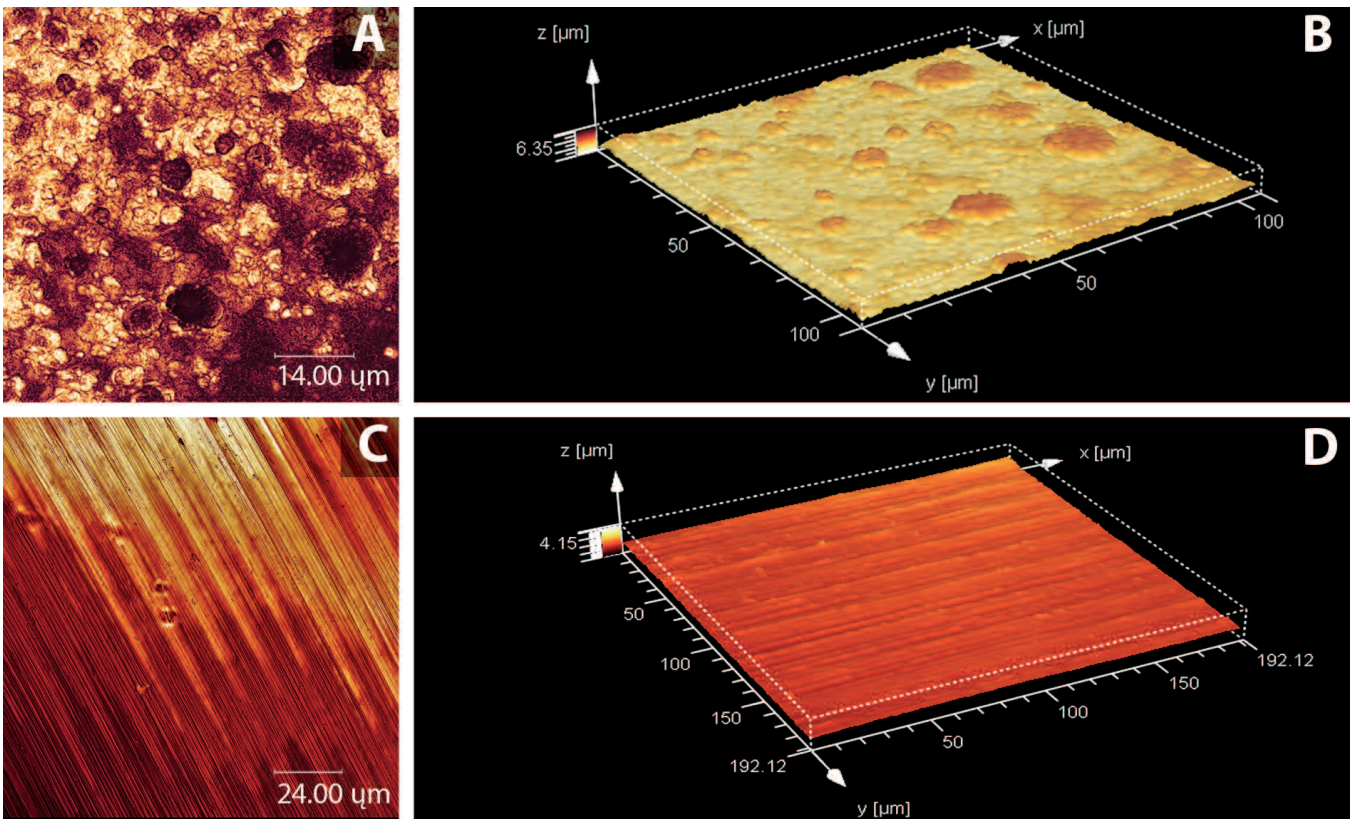

Fig. 1. A. Confocal backscattered imaging of TiCP rough surface (Osseotite®), showing the irregular distribution of peaks and caves that configure an irregular surface for bone cell attachment. **B.** Profilometric 3D reconstruction. In contrast, as shown in **C**, the machined surface presented parallel grooves that configure an almost uniform surface, quite regular in depth, as shown in the profilometric 3D reconstruction in **D**. In order to clarify interpretation of images, a glow LUT palette is presented, i.e. the darker zones are the deeper ones.

clustering or significant polarization around contact sites were observed, and SD values (Table 1) confirmed quite a similar mitochondrial distribution to that displayed in the control group, where osteoblasts, which adhere to glass surface, showed scattered mitochondria unevenly distributed. There is also a filamentous network of

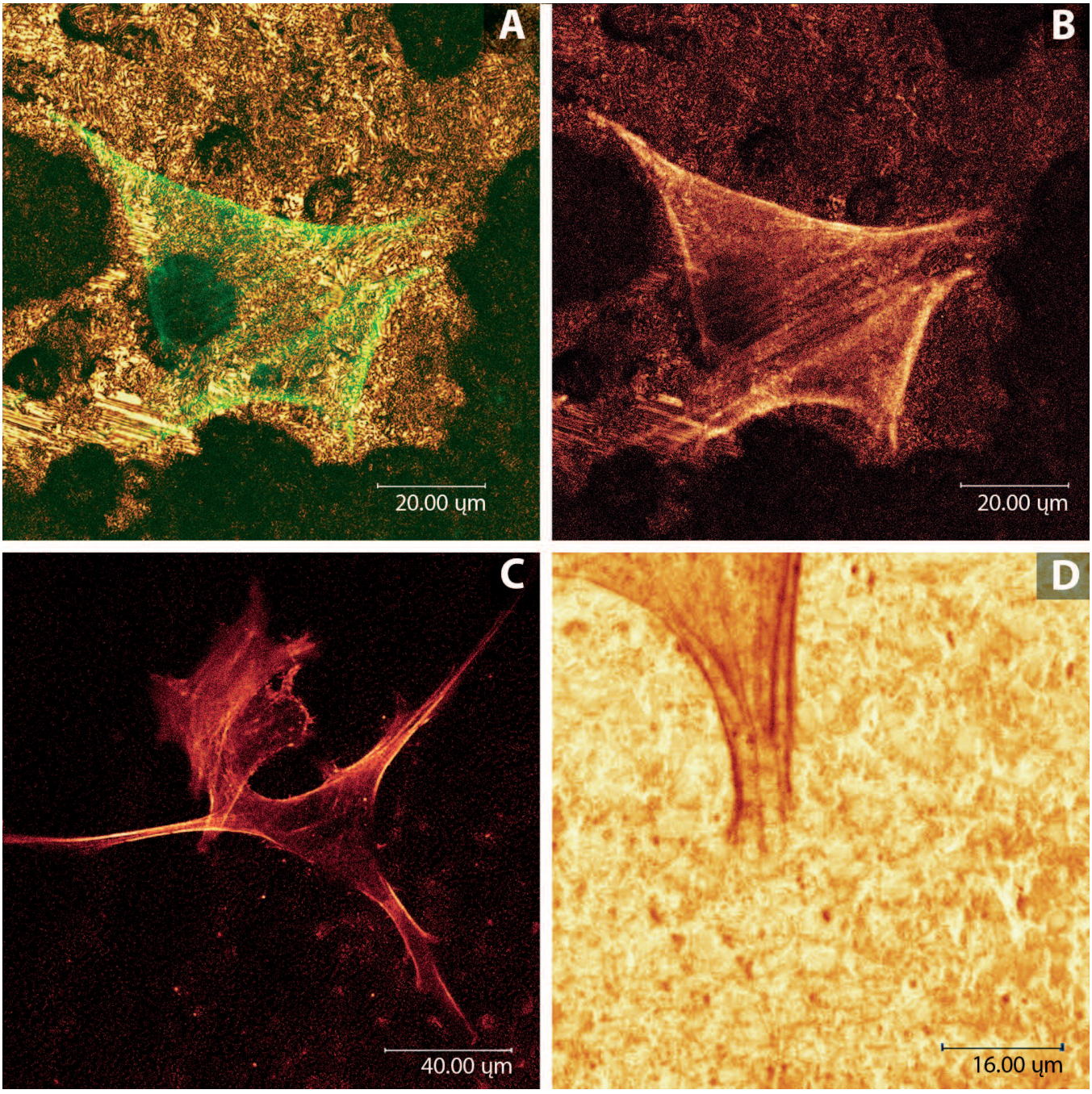

Fig. 2. A. Simultaneous imaging of disk surface and rhodamine-phalloidin stained NHOst® cell grown on the rough surface for 48 h. Cells fitted to the surface with the emission of filopodia and lamellipodia. As shown in **B**, when glow imaging was employed, the distribution and concentration of actin stress fibers is conditioned by surface irregularities. **C.** Merged image obtained from a serial acquisition of 50 stacks in the xyz mode, combining backscattered and fluorescence imaging. Long filopodia emitted from the cell body are looking for appropriate adhesion sites. **D.** Detailed image of a so called "cell foot" in a focal adhesion site, with actin stress fibers clearly polarized to the disk surface. In this case, an inverted glow palette is presented.

polarized mitochondria surrounding the nucleus (Fig. 6).

Statistical analysis

When analyzing the variable area of the selected ROIs, a highly significant difference ($p<2•E-10$) appeared between cells grown on the different surfaces tested, and cells growing on the rough, TiCP Osseotite® surface, showed the highest values, followed by cells growing on glass surface and finally, the smallest ones,

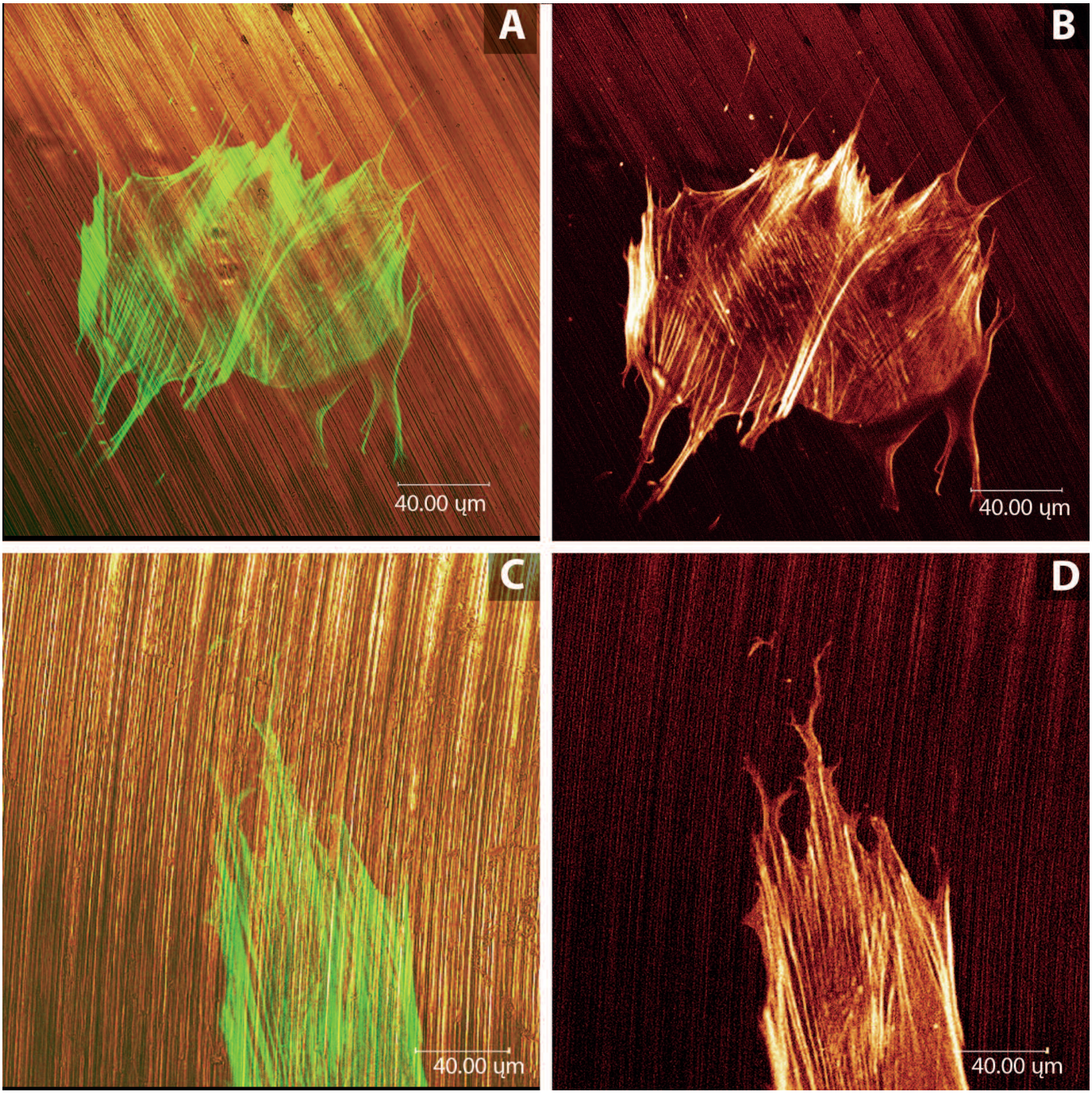

Fig. 3. A Simultaneous imaging of disk surface and rhodamine-phalloidin stained NHOst® cell grown on the machined surface for 48 h. Cells are predominantly flat and stress fibers run in diverse directions, as clearly shown in **B** when glow imaging was employed. In this case, cells are growing crossing over the grooves in a perpendicular way, with a discrete emission of filopodia. **C.** Some other cells growing in parallel to machined grooves with stress fibers covering the whole cell body, as highlighted in **D**.

cells growing on the machined surface. Despite this fact, the differences between red pixel means between groups were not significant (p=0.369). On the contrary, highly significant differences were found when comparing standard deviations (p<2•E-14), and skewness (p=0.011) (Table 1).

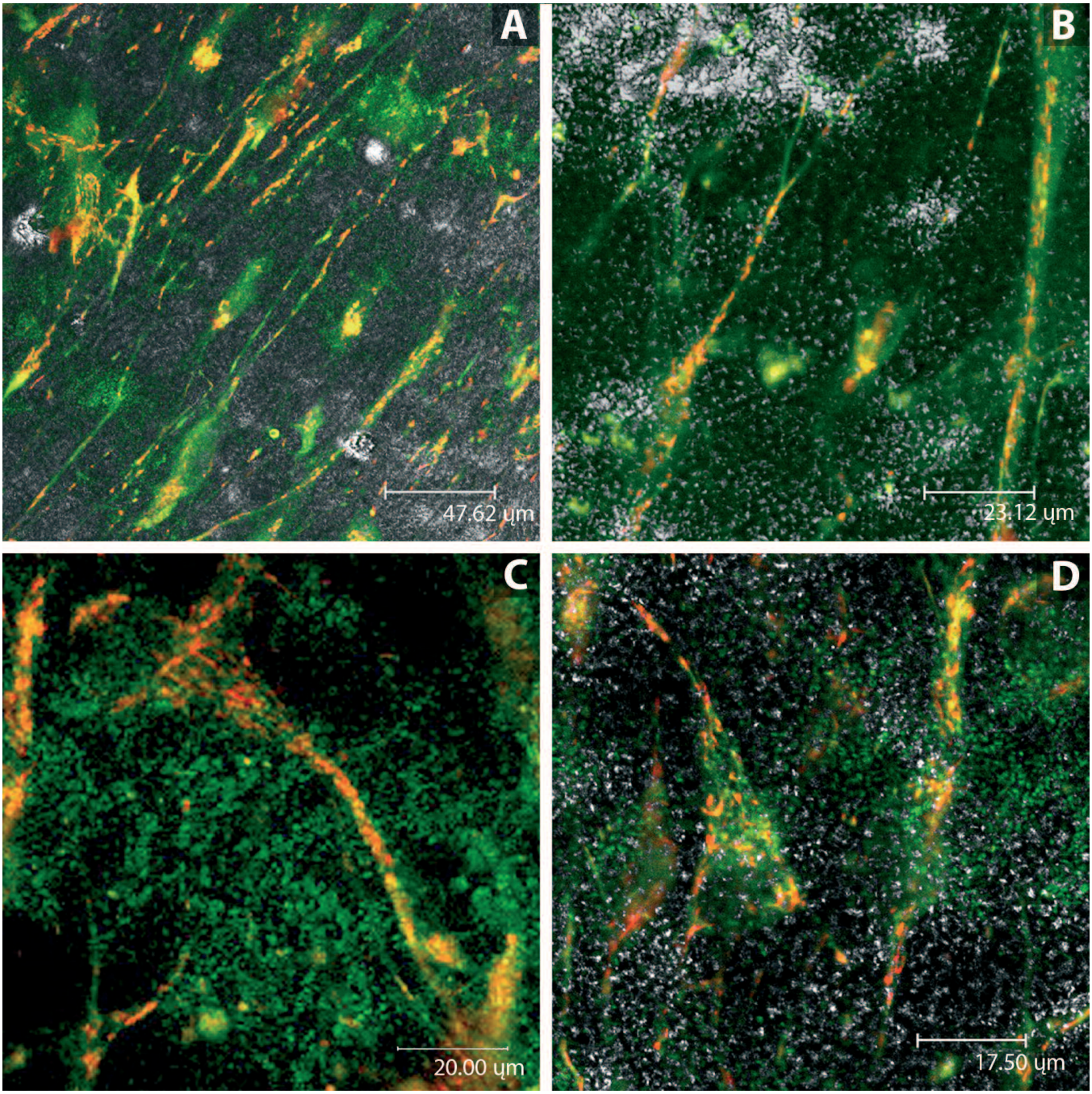

Fig. 4. A. Living cell imaging of JC1 stained osteoblasts simultaneously acquired with the backscattered imaging of Osseotite® disk surface 48 h after seeding. Cells emitted long protrusions in search of surface protuberancies. In red, highly energized mitochondria that accumulate in focal adhesion sites. **B.** Shown in detail, long filopodia are branching to contact with surface peaks, which appear in clear grey. Red stained mitochondria cluster in the energy requirement zones. **C.** The cell shows the typical morphology observed in the Osseotite® group, with long filopodial emission full of highly energized mitochondria, fitting to disk surface, in green. **D.** Mitochondrial clustering, red, in focal adhesion sites. Cells show an elongated morphology determined by relative surface peaks.

The results for post-hoc comparisons between groups, analyzing the differences in model-predicted means, are shown in Table 2. Briefly, highly significant differences were found in cell area when comparing the rough, Osseotite®, and machined groups with the control group, but not when comparing Osseotite® and machined groups. Significant differences between all three groups appeared when comparing standard

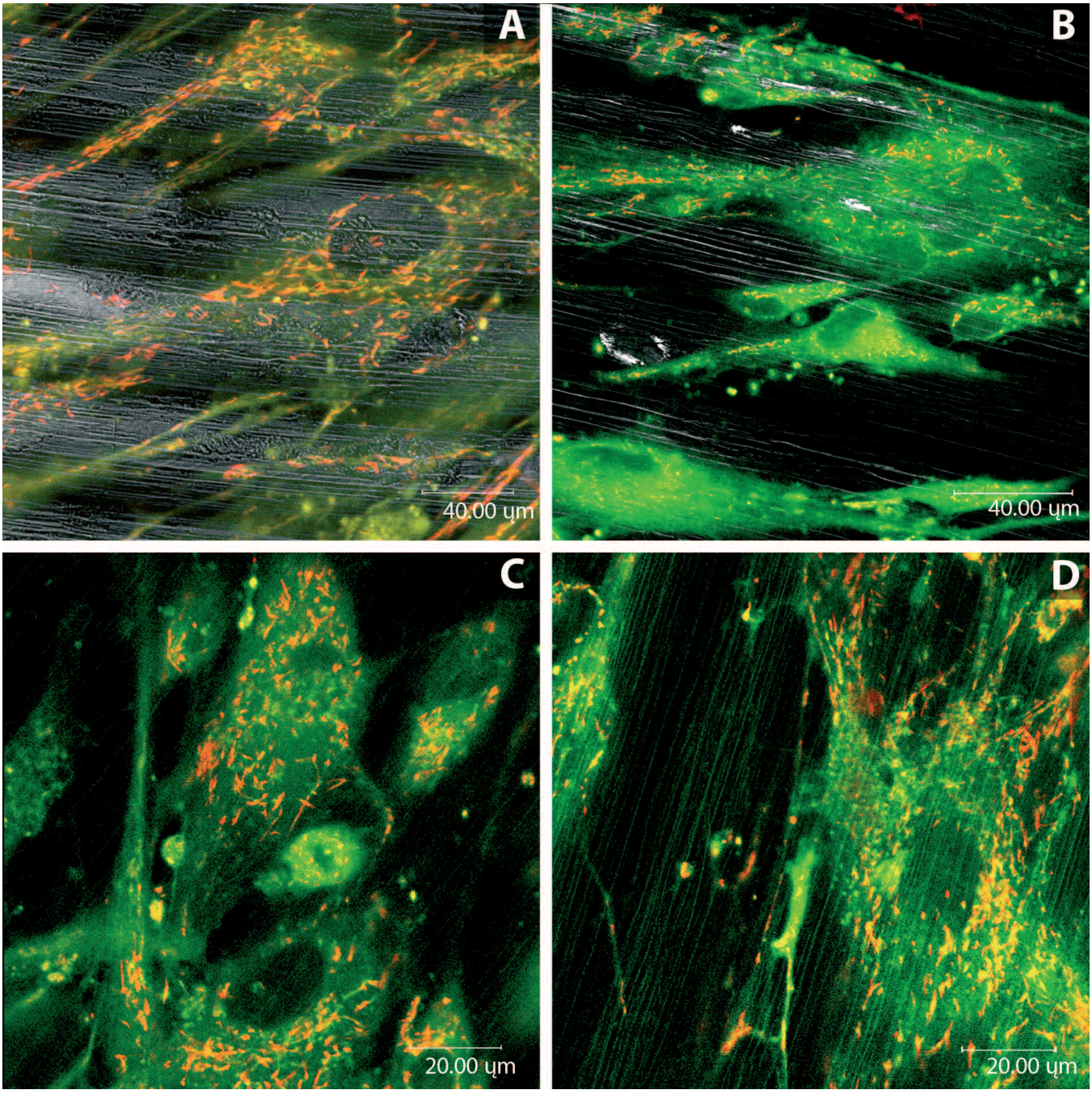

Fig. 5. A. Living cell imaging of JC1 stained osteoblasts simultaneously acquired with the backscattered imaging of the machined disk surface 48 h. after seeding. Cells are predominantly flat, and highly energized mitochondria, in red, are distributed along the cell body. **B.** Osteoblasts grown on the machined surface, with a relatively high cellular density that oriented along the grooves, some of the cells emitting small filopodia with low presence of red stained mitochondria. **C.** Polygonal osteoblasts growing on the machined surface. The cellular density is high, but no clear adhesion sites are observed. Highly energized mitochondria are scattered along the cell body. **D.** Shown in detail, combined backscattered image of machined disks clearly showing the grooved pattern and JC1 stained cells. Mitochondria are distributed near prolongations but also in the cell body. Cells appear to be flat and spread.

deviations for red pixel distribution, mainly when comparing cells growing on Osseotite® disks with the remaining groups. Statistically significant differences between Osseotite® and machined groups were found when comparing skewness of red pixel distribution, but not when comparing machined or Osseotite® groups with the control group.

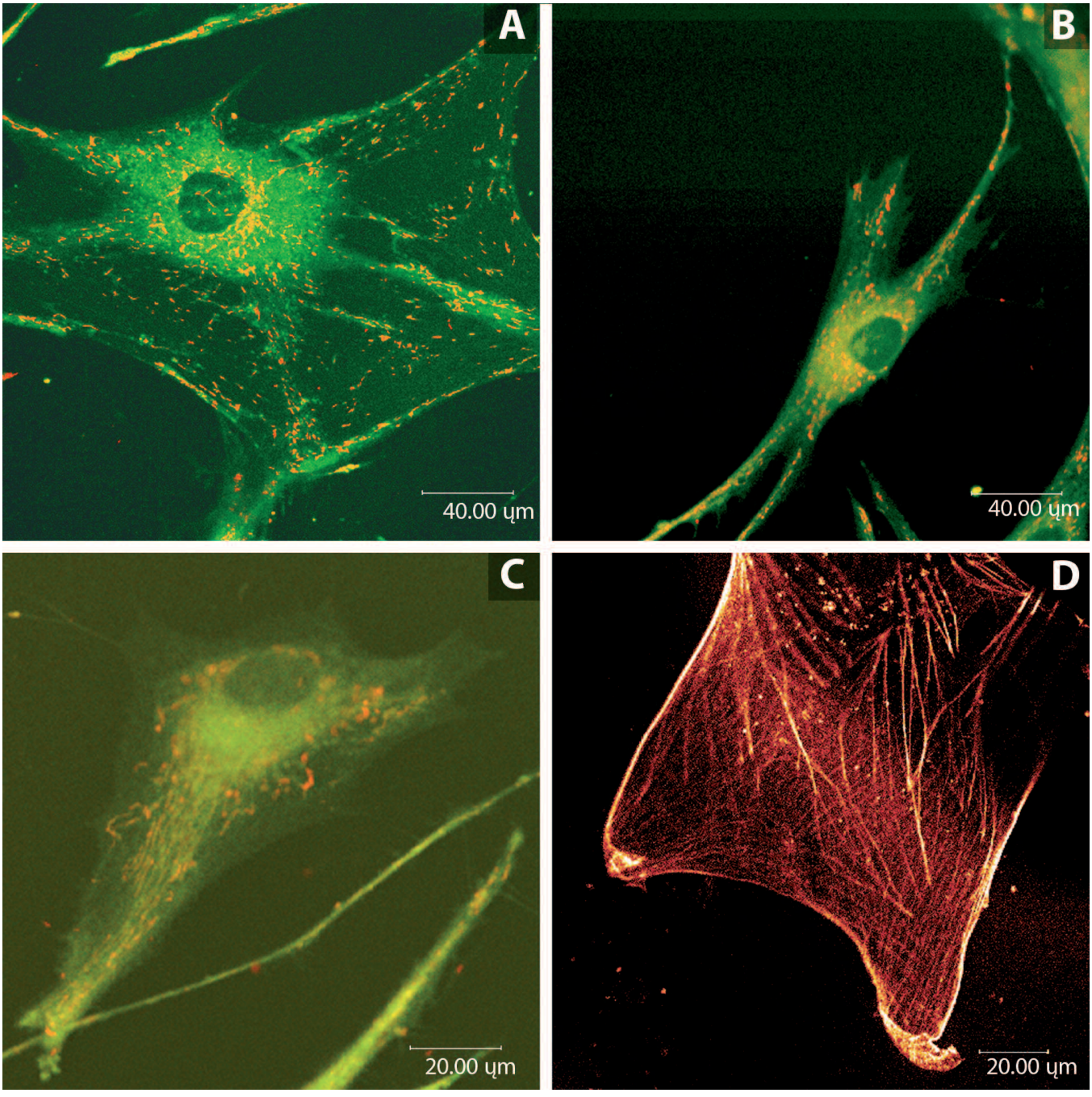

Fig. 6. A. Control cells growing on a glass surface and JC1 stained after 48h. Cell morphology reveals a non-polarized spreading in the search of differentiation cues. Highly energized mitochondria are scattered and unevenly distributed. In **B**, an elongated osteoblast growing on glass is emitting filopodia with highly energized mitochondria. Due to the absence of surface signaling, cell morphology is diverse, as shown also in **C**, where the cellular body adopted a nearly polygonal shape and mitochondria scatter along the cell. **D**. Rhodamine-phalloidin stained NHOst® cell growing on glass. Actin fibers are irregularly distributed along the cell body.

Table 1. Descriptive parameters for analyzed variables.

ROIs	Variables	Mín	Max	Mean	(CI 95%)
TiCP Machined	Area	145.86	4164.27	1046.37	(895.06; 1197.08)
N=110	Mean red pixels intensity	24.32	158.93	84.59	(79.41; 89.77)
	S.D. red pixels	20.81	86.39	46.74	(94.15; 49.32)
	Skewness red pixels	-.10	3.27	1.57	(1.47; 1.66)
TiCP Osseotite®	Area	212.19	2654.83	661.97	(540.67; 783.27)
N=61	Mean red pixels intensity	19.27	118.22	79.55	(72.42; 86.68)
	S.D. red pixels	9.14	57.16	28.79	25.58; 32.00)
	Skewness red pixels	0.63	3.73	1.86	(1.68; 2.03)
Controls	Area	165.65	9133.37	2744.09	(1924.92; 3563.26)
N=41	Mean red pixels intensity	52.06	122.68	86.12	(80.30; 91.93)
	S.D. red pixels	19.67	63.93	40.03	(36.07; 43.99)
	Skewness red pixels	0.70	3.74	1.69	(1.47; 1.91)

Table 2. Pairwise differences between groups with 95% confidence interval.

Variables	Surface A	Surface B	Mean Diff. (A-B)	p	CI 95%	
Area	Control	TiCP Machined	1697.72(*)	.000	1136.5734	2258.8644
		TiCP Osseotite	2082.12(*)	.000	1462.7920	2701.4418
	TiCP Machined	Osseotite	384.40	.155	-105.1689	873.9650
S.D. red pixels	Control	TiCP Machined	-6.70(*)	.016	-12.3802	-1.0247
		TiCP Osseotite	11.24(*)	.000	4.9784	17.5113
	TiCP Machined	TiCP Osseotite	17.95(*)	.000	12.9938	22.9008
Skewness red pixels	Control	TiCP Machined	.13	.502	-.1387	.3901
		TiCP Osseotite	-.17	.354	-.4624	.1214
	TiCP Machined	TiCP Osseotite	-.30(*)	.008	-.5269	-.0655

Discussion

The actin cytoskeleton is a dynamic structure that participates in cellular functions, including the maintenance of cell polarity and morphology, intracellular trafficking of organelles, cell motility, cell division and cell adhesion, providing structural support for cellular protrusions, including filopodia and lamellipodia (Zimmerman et al., 2004; Boldogh and Pon, 2006; Faghihi et al., 2007).

We have previously demonstrated that osteoblastic adhesion is significantly different on the two commonly and successfully used orthopedic biomaterials (Salido et al., 2007b; Vilches et al., 2007). On smooth surfaces, Ti CP machined, bone cells were predominantly planar, with stress fibers running in all directions, and thin filopodia, even when cells were aligned in parallel to the direction of the grooves. In contrast, on TiCP Osseotite® surfaces, the osteoblastic cells with elongated morphology, clearly defined wide lamellipodia and long filopodia displayed enhanced expression of stress fibers, and were able to form large clear focal contacts with the rough surface. These events support an active role for the biomaterial surface in the events that govern osteoblastic cell maturation.

Recently, studies have been made to understand the smooth/rough surface efficacies on phenotypic expressions on osteoblasts, in which a rough surface permits the attachment of more cells than a smooth surface (Komarova et al., 2000; Lim et al., 2007; Le Guéhennec et al., 2007; Popat et al., 2007; Khang et al., 2008). According to Biggs, osteoblast function and differentiation has recently been shown to be regulated to a high degree by adhesion and subsequent cellular spreading (Biggs et al., 2007). It has also been reported that cell shape and cytoskeleton alignment was with respect to the surface topography of grooved surface, which also seems to have a profound influence on osteogenesis (Jayaraman et al., 2004; Masaki et al., 2005; Hata et al., 2007; Zhao et al., 2007).

Interactions of mitochondria with the different cytoskeletal networks are essential for the maintenance of mitochondrial function, with their capital role in the production of the largest part of cellular ATP needed for endoergonic processes, movement and anchorage within the cells (Boldogh and Pon, 2007).

Mitochondrial bioenergetic assessment in living normal human NHOst® osteoblasts, stained with JC1, growing on the different test surfaces allowed us to correlate the mitochondrial distribution with the substratum microtopography. In the irregular substratum, full of peaks and caves, mitochondrial polarization is related to selected anchorage points, while in machined surfaces, highly energized mitochondria, unevenly distributed, filled the cell body. In this sense, statistically significant differences between rough and machined

surfaces were established.

As recently described by von Braun, mitochondria are able to move, ensuring a positioning of the organelle close to the place where its function is required (von Braun and Schleiff, 2007).The selective retention of mitochondria may, thus, enrich the organelle responsible for energy production at sites of high energy demand. Boldogh has demonstrated the role of the cytoskeleton in retention of mitochondria at sites of high ATP utilization within neurons, and an immobilization of mitochondria at sites of NGF stimulation has also been described (Anesti and Scorrano, 2006; Boldogh and Pon, 2006, 2007).

The results presented herein demonstrate how surface topography conditions the mitochondrial distribution in living NHOst® cells, and also that this polarization follows the actin patterns that we have previously described (Chen et al., 2003; Appaix et al., 2003; Luthen et al., 2005; Ghosh and Ingber, 2007; Salido et al., 2007b). Cycles of polarization based on the directional flow of actin and plasma membrane have long been proposed as the mechanism that enables motile cells to crawl, in response to effective concentrations of chemoattractans that trigger actin polymerization at the leading edge to push the cell forward. In consonance with our results for cells growing on rough surfaces, a recent publication by Sanchez-Madrid described a redistribution of mitochondria towards the uropod of polarized migrating leukocytes (Sanchez-Madrid and Serrador, 2007). Conversely, mitochondrial distribution in planar cells growing on machined surfaces reveals quite a different response, clearly confirmed when comparing standard deviation ($p<2.E14$) and skewness ($p=0.1111$) between groups. It is known that surface topography can induce mechanical forces that are transduced into a biochemical response, thus building the molecular basis of mechanotransduction, a process where high amounts of energy are demanded (Ingber, 2003a,b; Dalby, 2005; Frederick and Shaw, 2007). According to recent studies, mitochondria with normal membrane potential exhibit the higher level of anterograde transport in neurons. Consistent with this, mitochondria that accumulate at sites of presynaptic development exhibit higher membrane potential compared with mitochondria that are not at those sites (Boldogh and Pon, 2007). In view of our results, we can postulate that, in the normal human osteoblastic cells tested, the establishment of the most effective focal adhesion sites needs high energy requirements similar to the active growth cones of neurons.

Finally, with respect to the methodology employed, we have chosen the confocal microscope as an extremely useful tool that incorporates important advances in microscopy, which have enabled the imaging of intact, optically nontransparent specimens to produce high resolution images of cells and tissues with the use of fluorescent probes (Udupa et al, 2000; Voytik-Harbin et al., 2003; Tan et al., 2004, 2007; Vilches et al., 2007; Gatti et al., 2008). As we have shown in this paper, the combined use of reflectance and fluorescence modes is of high interest to provide detailed images of living cell interactions with underlying surfaces in biomedical devices. The methodology described by our group herein is useful to directly visualize and quantify the role of underlying environmental cues for force-generating and anchoraging activities on mitochondrial bioenergetics in living cells growing on a number of customized biomaterial surfaces.

Conclusion

We have demonstrated, for the first time to our knowledge, using living NHOst® cells, that the rough microtopography conditions a more precise energy requirement than smooth and machined surfaces do, in terms of mitochondrial bioenergetics. In our opinion, the polarization of energized mitochondria around effective focal adhesion sites, in response to biomaterial induced cues, is an indicator of a better cellular anchorage and adhesion that, undoubtedly, improves the first stages of the osseointegration process. The combination of backscattered and fluorescence confocal imaging of living cells and underlying surfaces, employed in the study, becomes a valuable tool for testing the efficiency of biomaterials design.

Acknowledgements. This work has been supported by a FIS 05/1816 grant from Instituto de Salud Carlos III, Spain. The authors want to acknowledge Dr. Torres Lagares for kindly providing the titanium disks prefabricated by 3i (Palm Beach Gardens, USA). We also thank the pregraduate student Ramiro Petre for the technical collaboration.

References

Anesti V. and Scorrano L. (2006). The relationship between mitochondrial shape and function and the cytoskeleton. Biochim. Biophys. Acta 1757, 692-699.

Appaix F., Kuznetsov A.V., Usson Y., Kay L., Andrienko T., Olivares J., Kaambre T., Sikk P., Margreiter R. and Saks V. (2003). Possible role of cytoskeleton in intracellular arrangement and regulation of mitochondria. Exp. Physiol. 88, 175-190.

Biggs M.J., Richards R.G., Gadegaard N., Wilkinson C.D. and Dalby M.J. (2007). The effects of nanoscale pits on primary human osteoblast adhesion formation and cellular spreading. J. Mater. Sci. Mater. Med. 18, 399-404.

Boldogh I.R. and Pon L.A. (2006). Interactions of mitochondria with the actin cytoskeleton. Biochim. Biophys. Acta 1763, 450-462.

Boldogh I.R. and Pon L.A. (2007). Mitochondria on the move. Trends Cell. Biol. 17, 502-510.

Chen C.S., Alonso J.L., Ostuni E., Whitesides G.M. and Ingber D.E. (2003). Cell shape provides global control of focal adhesion assembly. Biochem. Biophys. Res. Commun. 307, 355-361.

Chiesa R., Giavaresi G., Fini M., Sandrini E., Giordano C, Bianchi A. and Giardino R. (2007). In vitro and in vivo performance of a novel surface treatment to enhance osseointegration of endosseous implants. Oral Surg. Oral Med. Oral Pathol. Oral Radiol. Endod. 103, 745-756.

Dalby M.J. (2005). Topographically induced direct cell

mechanotransduction. Med. Eng. Phys. 27, 730-742.

Dedov V.N. and Roufogalis B.D. (1999). Organisation of mitochondria in living sensory neurons. FEBS Lett. 456, 171-174.

Diener A., Nebe B., Lüthen F., Becker P., Beck U., Neumann H.G. and Rychly J. (2005). Control of focal adhesion dynamics by material surface characteristics. Biomaterials 26, 383-392.

Faghihi S., Azari F., Zhilyaev A.P., Szpunar J.A., Vali H. and Tabrizian M. (2007). Cellular and molecular interactions between MC3T3-E1 pre-osteoblasts and nanostructured titanium produced by high-pressure torsion. Biomaterials 28, 3887-3895.

Frederick R.L. and Shaw J.M. (2007). Moving mitochondria: establishing distribution of an essential organelle. Traffic 8, 1668-1675.

Gatti R., Orlandini G., Uggeri J., Belletti S., Galli C., Raspanti M., Scandroglio R. and Guizzardi S. (2008). Analysis of living cells grown on different titanium surfaces by time-lapse confocal microscopy. Micron 39, 137-143.

Ghosh K. and Ingber D.E. (2007). Micromechanical control of cell and tissue development: implications for tissue engineering. Adv. Drug. Deliv. Rev. 10, 1306-1318.

Grigoriou V., Shapiro I.M., Cavalcanti-Adam E.A., Composto R.J., Ducheyne P. and Adams C.S. (2005). Apoptosis and survival of osteoblast-like cells are regulated by surface attachment. J. Biol. Chem. 280, 1733-1739.

Hata K., Ikebe K., Wada M. and Nokubi T. (2007). Osteoblast response to titanium regulates transcriptional activity of Runx2 through MAPK pathway. J. Biomed. Mater. Res. A. 81, 446-452.

Hu K., Ji L., Applegate K.T., Danuser G. and Waterman-Storer C.M. (2007). Differential transmission of actin motion within focal adhesions. Science 315, 111-115.

Ingber D.E. (2003). Mechanosensation through integrins: cells act locally but think globally. Proc. Natl. Acad. Sci. USA 100, 1472-1474.

Ingber D.E. (2003a). Tensegrity I. Cell structure and hierarchical systems biology. J. Cell Sci. 116, 1157-1173.

Ingber D.E. (2003b) Tensegrity II. How structural networks influence cellular information processing networks. J. Cell.Sci. 116, 1397-1408.

Jayaraman M., Meyer U., Bühner M., Joos U. and Wiesmann H.P. (2004). Influence of titanium surfaces on attachment of osteoblast-like cells in vitro. Biomaterials 25, 625-631.

Khang D., Lu J., Yao C., Haberstroh K.M. and Webster T.J. (2008). The role of nanometer and sub-micron surface features on vascular and bone cell adhesion on titanium. Biomaterials 29, 970-983.

Komarova S.V., Ataullakhanov F.I. and Globus R.K. (2000). Bioenergetics and mitochondrial transmembrane potential during differentiation of cultured osteoblasts. Am. J. Physiol. Cell. Physiol. 279, C1220-1229.

Le Guéhennec L., Soueidan A., Layrolle P. and Amouriq Y. (2007). Surface treatments of titanium dental implants for rapid osseointegration. Dent. Mater. 23, 844-854.

Lim J.Y., Dreiss A.D., Zhou Z., Hansen J.C., Siedlecki C.A., Hengstebeck R.W., Cheng J., Winograd N. and Donahue H.J. (2007). The regulation of integrin-mediated osteoblast focal adhesion and focal adhesion kinase expression by nanoscale topography. Biomaterials 28, 1787-1797.

Lüthen F., Lange R., Becker P., Rychly J., Beck U. and Nebe J.G. (2005). The influence of surface roughness of titanium on beta1-and beta3-integrin adhesion and the organization of fibronectin in human osteoblastic cells. Biomaterials 26, 2423-2440.

Masaki C., Schneider G.B., Zaharias R., Seabold D. and Stanford C. (2005). Effects of implant surface microtopography on osteoblast gene expression. Clin. Oral Implants Res. 16, 650-656.

Pierres A., Benoliel A.M. and Bongrand P. (2002). Cell fitting to adhesive surfaces: A prerequisite to firm attachment and subsequent events. Eur. Cell. Mater. 30, 31-45.

Popat K.C., Leoni L., Grimes C.A. and Desai T.A. (2007). Influence of engineered titania nanotubular surfaces on bone cells. Biomaterials 28, 3188-3197.

Sader M.S., Balduino A., Soares G. de A. and Borojevic R. (2005). Effect of three distinct treatments of titanium surface on osteoblast attachment, proliferation, and differentiation. Clin. Oral Implants Res. 16, 667-675.

Salido M., Gonzalez J.L. and Vilches J. (2007a). Loss of mitochondrial membrane potential is inhibited by bombesin in etoposide-induced apoptosis in PC3 prostate carcinoma cells. Mol. Cancer Ther. 6, 1292-1299.

Salido M., Vilches J.I., Gutiérrez J.L. and Vilches J. (2007b). Actin cytoskeletal organization in human osteoblasts grown on different dental titanium implant surfaces. Histol. Histopathol. 22, 1355-1364.

Salvioli S., Ardizzoni A., Franceschi C. and Cossarizza A. (1997). JC-1, but not DiOC6 (3) or rhodamine 123, is a reliable fluorescent probe to assess delta psi changes in intact cells: implications for studies on mitochondrial functionality during apoptosis. FEBS Lett. 411, 77-82.

Sanchez-Madrid F. and Serrador J.M. (2007). Mitochondrial redistribution: adding new players to the chemotaxis game. Trends Immunol. 28, 193-196.

Tan W., Sendemir-Urkmez A., Fahrner L.J., Jamison R., Leckband D. and Boppart S.A. (2004). Structural and functional optical imaging of three-dimensional engineered tissue development. Tissue Eng. 10, 1747-1756.

Tan W., Vinegoni C., Norman J.J., Desai T.A. and Boppart S.A. (2007). Imaging cellular responses to mechanical stimuli within three-dimensional tissue constructs. Microsc. Res. Tech. 70, 361-371.

Udupa G., Singaperumal M., Sirohi R.S. and Kothiyal M.P. (2000). Characterization of surface topography by confocal microscopy: I. Principles and the measurement system. Meas. Sci. Technol. 11, 305-314.

Vilches J., Vilches-Perez J.I. and Salido M. (2007). Cell-surface interaction in biomedical implants assessed by simultaneous fluorescence and reflection confocal microscopy. In: Modern research and educational topics in microscopy. Mendez Vilas (ed). Formatex. Badajoz. pp 60-67.

von Braun S.S. and Schleiff E. (2007). Movement of endosymbiotic organelles. Curr. Protein Pept. Sci. 8, 426-438.

Voytik-Harbin S.L., Roeder B.A., Sturgis J.E., Kokini K. and Robinson J.P. (2003). Simultaneous mechanical loading and confocal reflection microscopy for three-dimensional microbiomechanical analysis of biomaterials and tissue constructs. Microsc. Microanal. 9, 74-85.

Zhao G., Raines A.L., Wieland M., Schwartz Z. and Boyan B.D. (2007). Requirement for both micron- and submicron scale structure for synergistic responses of osteoblasts to substrate surface energy and topography. Biomaterials 28, 2821-2829.

Zimerman B., Arnold M., Ulmer J., Blümmel J., Besser A, Spatz J.P. and Geiger B. (2004). Formation of focal adhesion-stress fiber complexes coordinated by adhesive and non-adhesive surface domains. IEE. Proc. Nanobiotechnol. 151, 62-66.

Accepted May 8, 2009